Screen-Printed Capacitive Tactile Sensor For Monitoring Tool-Tissue Interactions and Grasping Performances of a Surgical Magnetic Microgripper

D. Anastasia Aubeeluck[1], Cameron Forbrigger[1], Sara Mohseni Taromsari[1], Tianhao Chen[2], Eric Diller[1,3] and Hani E. Naguib*[1,2,4]

[1]Department of Mechanical and Industrial Engineering, University of Toronto, 5 King's College Road, Toronto M5S 3G8, Canada

[2]Institute of Biomedical Engineering, University of Toronto, 164 College Street, Toronto, Ontario, M5S 3G9, Canada

[3]University of Toronto Robotics Institute, University of Toronto Engineering, 55 St. George Street Toronto, Ontario, M5S 1A4, Canada

[4]Toronto Rehabilitation Institute, 550 University Ave, Toronto, Ontario, M5G 2A2, Canada

* Email: naguib@mie.utoronto.ca

ABSTRACT – With miniaturization and wireless actuation for a class of magnetic microgripper for robot-assisted minimally invasive endoscopic intraventricular surgery, surgeons are unable to acquire tactile sensory information of tissues and organs during tool-tissue manipulation and grasping tasks. To minimize the risks of tissue trauma and improve surgical performance, surgeons require haptic feedback technologies to be integrated onto micro-scale surgical tools for tactile information. However, current sensors cannot be equipped onto the interior jaw of the microgripper due to low pressure range and small scale criteria for RMIS implementation for pediatric neurosurgery. This study proposes a 24 mm^2, ultra-thin and flexible capacitive tactile sensor for the interior jaws of a disposable surgical magnetically-controlled microgripper to potentially monitor and regulate tool-tissue manipulation pressures/forces in real-time to improve grasping performances and quality of surgical procedures. To lower fabrication costs, the multiple layers of the capacitive sensor were screen-printed and assembled to produce a 100 µm thick sensor. To enhance range and sensitivity, four different morphologies were developed for the dielectric layer and integrated into the sensor design. The dielectric layers were fabricated by optimizing and processing TPU into a suitable ink adequate for screen printing large surfaces and microstructures. The final optimized capacitive tactile sensor with a grid-like micro-structured dielectric design's electromechanical performance was modelled as a bi-linear response with two sensitivity modes for a sensing range of 0.42 – 54.2 kPa (0.01 - 1.30 N applied on 24 mm^2 of gripper jaw). The results also indicated performance comparable to more expensive tactile sensors with a hysteresis of 8.8% and a repeatable response to applied cycling loadings with a maximum response signal decay of 1.85%. This study highlights that simple screen printing method can be used as a low-cost alternative to fabricate high performance tactile sensors to be integrated to the interior jaw of the microgripper designed for disposable endoscopic intraventricular surgeries.

KEYWORDS: Robot-assisted minimally invasive surgery, capacitive tactile sensor, flexible electronic devices, screen printing, morphology of dielectric (microstructure)

1. Introduction

In the wake of the advancement of robot-assisted minimally invasive surgeries (RMIS) for neurosurgery, safer and more efficient manipulation of sensitive brain tissues is imperative while exposing or gaining access to otherwise obstructed parts of the brain to reduce trauma and surgical brain injuries to patients[1]. RMIS for neurosurgery aims to lower recovery time, risks of infection and pain in patients, and to reduce incision size[2,3,4]. To perform RMIS surgical procedures, miniaturized robotic grippers inserted through narrow working channels are used to grasp and pull soft tissues by using a combination of pinch forces (normal force) and frictional shear forces[1].

For application in RMIS for pediatric neuroendoscopy with narrower working channels, Lim et al. and Forbrigger et al. proposed a novel magnetic microgripper (of diameter 4 mm as shown in Figure 1 (a)) with grasping capabilities and an interior gripper jaw area of 24 mm^2 [2,5,6]. This tool is designed to be capable of performing micro-scale surgical incision and retraction (pulling apart) procedures with grasping forces up to 0.181 N (7.54 kPa) for intraventricular neurosurgery, namely tumor resection via magnetic actuation[5,6]. Magnetic actuation of the microgripper is biocompatible, wireless and offers greater miniaturization for RMIS applications[2,5,6]. However, owing to miniaturization, the microgripper requires larger displacement to generate a larger magnitude of grasping forces to perform surgical operations similar to conventional larger grippers[5,7]. Furthermore, based on literature, grasping force errors due to too little or too large force exerted by surgical grippers can cause tissue slippage or tissue damage[1]. Thus, surgeons must acquire and monitor tactile sensory information during RMIS tool navigation and grasping[7].

During conventional surgeries and with non-robotic surgical grippers, tactile feedback is acquired directly by surgeons through tool grasp and palpation[3,4]. For RMIS with magnetic robotic grippers, surgeons have no direct contact with the tool due to spatial constraints and wireless actuation. Thus, they are unable to acquire tactile sensory information of tissues and organs during tool-tissue manipulation which increases tissue trauma risks and associated complications[3,4,6,8]. To ensure safety and efficiency of surgical operations, tactile haptic feedback technologies must be equipped to surgical tools to relay tactile and force information to surgeons in RMIS in real-time[4,7,8]. Moreover, haptic feedback could be used to optimize wireless magnetic actuation of the microgripper to increase precision and efficiency by monitoring and regulating grasping forces using a closed-loop control system[5]. Current tactile haptic feedback solutions cannot be integrated to the interior jaws of the magnetic microgripper due to misalignment, bulkiness, size limitations, RMIS working space constraint, and low force range requirements (0 to 1.35 N) based on neuroendoscopy procedures[9,10]. Gripper shape and size of micro-scale surgical tools are designed specifically for particular type of surgeries and, hence, require highly customized tactile sensors for haptic feedback both in terms of physical aspect and performance. Customized and high performance tactile sensors are generally associated with labor-intensive processes and high fabrication costs, thereby deterring implementation onto novel surgical tools especially with increasing demand for disposable tools for one-time surgical use[11,12,13,14].

To remedy haptic feedback limitations, this study proposes a 24 mm^2, ultra-thin and flexible capacitive tactile sensor (Sensing Area) for the interior jaws of a disposable surgical magnetically-controlled microgripper as shown in Figure 1 (a). Conductive tracks and connection pads are added for ease of data acquisition for sensor characterization and their design is not investigated in this study. The sensor can be used to potentially monitor and regulate tool-tissue manipulation pressures/forces in real-time to increase safety, improve grasping performances and quality of surgical procedures. The capacitive tactile sensor, shown on the surgical gripper in Figure 1 (b), comprises of two conducting parallel facing electrodes (with overlapping area A) separated by dielectric layers. The thickness, d, of the dielectric changes in response to a normal force load applied, while the area of superimposing electrodes is constant. This change in dielectric thickness between the electrodes results in a change of capacitance which can be used to interpret tactile information regarding pressure/force applied on the inner jaw surface of the microgripper. This capacitive transduction mode is chosen for the interior rigid surface of the gripper jaw over other sensing transduction mechanisms due to its linear response, high sensitivity, lower minimum detectable pressure, limited hysteresis, large dynamic pressure range, and compatibility for a relatively large sensing surface area[9]. Considering its processability into thin micro-structured films, low Young's modulus and dielectric properties, thermoplastic polyurethane (TPU) material was selected as part of the dielectric, spacer and liner layer in the sensor design[15]. A combination of TPU-air-TPU dielectric layer is chosen to potentially monitor and differentiate

detectable small and large pressure ranges (S_1 and S_2). Figure 1 (c) depicts the multiple sub-components of the proposed capacitive tactile sensor design. The selection of materials and structural design of the sensor's various components were based on weak diamagnetism to avoid interference with the magnetic actuation of the gripper, biocompatibility during tool-tissue interactions, and flexibility for ease of deformation for pressure sensing during surgery.

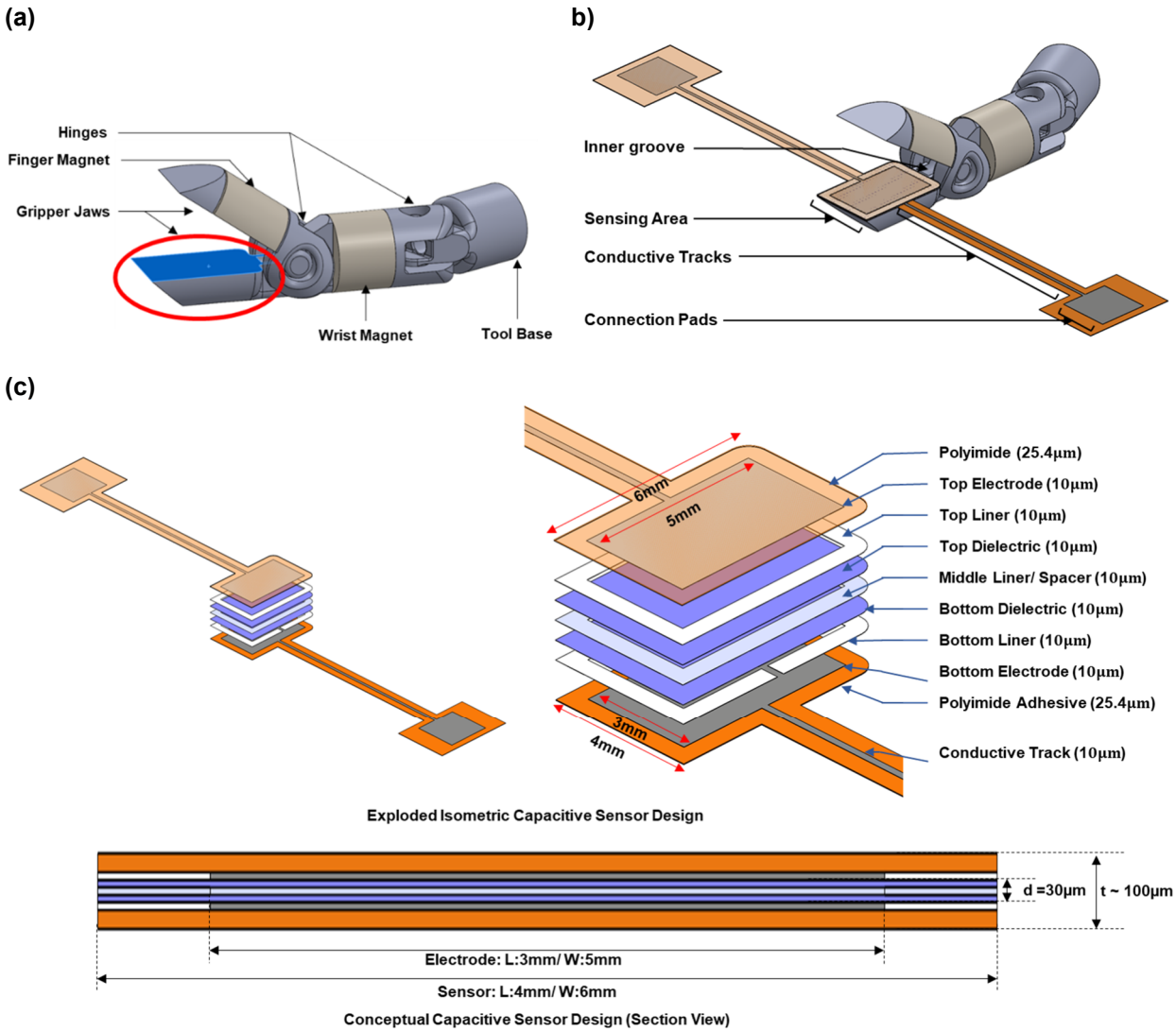

Figure 1. (a) CAD design of Magnetic Microgripper with a 24 mm^2 Surface Area of interior gripper jaw area. (b) CAD of 3D printed Magnetic Microgripper and capacitive tactile sensor, (c) Schematic illustration of multilayered capacitive tactile sensor design with a proposed sensing area *(A)* of 15 mm^2.

To improve sensor performance while maintaining the physical constraints for RMIS and the interior gripper jaw surface, this study specifically investigates the proposed sensor's electromechanical performance with various geometric morphologies for the dielectric layer of the sensor. The structural properties of elastomers as dielectric medium can affect sensor performance in terms of sensitivity and response time[16]. Hence, this study generated four different designs of micro-structured thin TPU dielectric layer (Design A, B, C and D) with varied structural properties to determine an improved dielectric morphology for the capacitive tactile sensor's performance. Micro-structured pressure and tactile sensors have been traditionally associated with chemical etching and photolithography technologies which require high fabrication costs, labor-intensive processes, costly chemicals, specialized equipment, and clean room facilities[13,16]. To meet size and fabrication limitations for disposable solutions, this study opted for screen printing technologies with optimized TPU ink. This approach facilitated the development and fabrication of ultra-thin, flexible, and micro-structured layers for the proposed capacitive tactile sensor to specifically acquire tactile feedback for a magnetic

microgripper during RMIS applications for neuroendoscopy procedures.

2. Experimental Section

2.1 Materials

Screen printable silver ink (Metalon® HPS-FG32 Silver Screen Ink) supplied by NovaCentrix was chosen for conductive tracks and electrodes. Kapton® Polyimide film with adhesive from McMaster-Carr was used as substrate and laminating agent. The chosen material for the dielectric, spacer and liner ink is Thermoplastic Polyurethane pellets (TPU - Pearlbond™ 12F75UV) with a dielectric constant of 4. It is supplied by Lubrizol Advanced Materials. The solvents used for dielectric ink formulation are N, N-dimethylformamide (DMF) and Tetrahydrofuran (THF) from Sigma Aldrich.

2.2 Fabrication of Sensor Sub-Components & Sensor Assembly

To formulate screen-printable dielectric ink, different weight percentages of TPU (10 wt%, 15 wt%, 20 wt%, 25 wt% and 30 wt%) were fabricated by dissolving TPU pellets in 1:1 ratio of THF and DMF solvents using magnetic stirring (70^{o}C at 500 RPM for 24 hours), as outlined in Figure 2 (a). Once a highly viscous ink solution was obtained, it was weighed multiple times to monitor evaporation of the solvent content. The ink was degassed in a vacuum, weighed and sealed to prevent solvent evaporation. Prior to verifying printability and proceeding with screen printing, the TPU ink solution was reheated to 70°C and stirred until ink softening while monitoring the ink's weight to maintain consistency.

Screen printing was performed using a manual 8 in. by 10 in. screen printer (Model MSP-088) along with emulsion screens (Hary Manufacturing Inc, New Jersey, USA). Customized patterns for the sub-components of capacitive sensor were prepared using AutoCAD (Autodesk, Inc., Mill Valley, CA) and implemented on stainless-steel screen printing mesh (mesh angle 22.5, 0.0005" emulsion thickness, 325 threads/in and wire diameter 0.009 in). The screen printing mesh and screen printer were then used to deposit patterned materials onto a substrate. For consistent screen printing, the snap-off height was set to 0.035 in., and the squeegee angle was maintained at 45 degrees. The squeegee pressure and speed ranged approximately from 0.2 to 0.5 kg and from 25 to 50 mm/s, respectively. The downward force applied by the squeegee blade onto the screen and substrate was monitored by measuring the weight using a balance. The speed of the squeegee across the screen was manually timed using a stopwatch to control consistent timing between each print stroke.

To fabricate the electrode layer and conductive tracks, screen printable silver ink was screen printed with a single stroke onto polyimide substrate and cured at 175°C for 5 minutes in an oven. The electrodes were designed using AutoCAD with a sensing area of 15 mm^2 (A) to allow for a 0.5 mm offset on the 24 mm^2 of the interior gripper jaw surface area for uniform pressure sensing and improved structural integrity for the sensor. The designs of the micro-structured dielectric, liner and spacer layer were also prepared using AutoCAD and then patterned onto screen frames. The dielectric, liner and spacer layer were screen printed onto their respective substrates with a single print stroke for the deposition of 10 µm of TPU material. The printed TPU materials were then allowed to air dry in a fume hood.

The assembly and screen-printing order process of the multiple layers of the capacitive sensors are outlined in Figure 2 (b). The top and bottom layers with the screen-printed materials were then superimposed such that the top electrode and bottom electrode area overlap and are separated by the dielectric medium (two layers of TPU and an air gap). The air gap is maintained by the TPU liner layer. Four different architectural designs of the dielectric TPU layer were generated based on the same thickness (d) and sensing area (A) to develop four different dielectric morphologies for the assembled capacitive sensor (Design A, B, C and D). Figure 2 (c) illustrates the varying surface morphologies of the dielectric designs, each using 100 µm line width microfeatures (Design A has no microfeatures. Design B consists of columns of 100 µm line widths of TPU with 100 µm spacing between each column. Design C features a grid design with columns and rows of 100 µm line widths of TPU, with 100 µm spacing between each column and row. Design D includes 100 µm diameter pillars of TPU with 100 µm spacing between each pillar). The layers were laminated and sealed using polyimide adhesive to insulate the conductive tracks, seal the content from human/patient contact for

biocompatibility, protect the assembly from humidity and maintain structural integrity of the multiple layers together during testing and characterization.

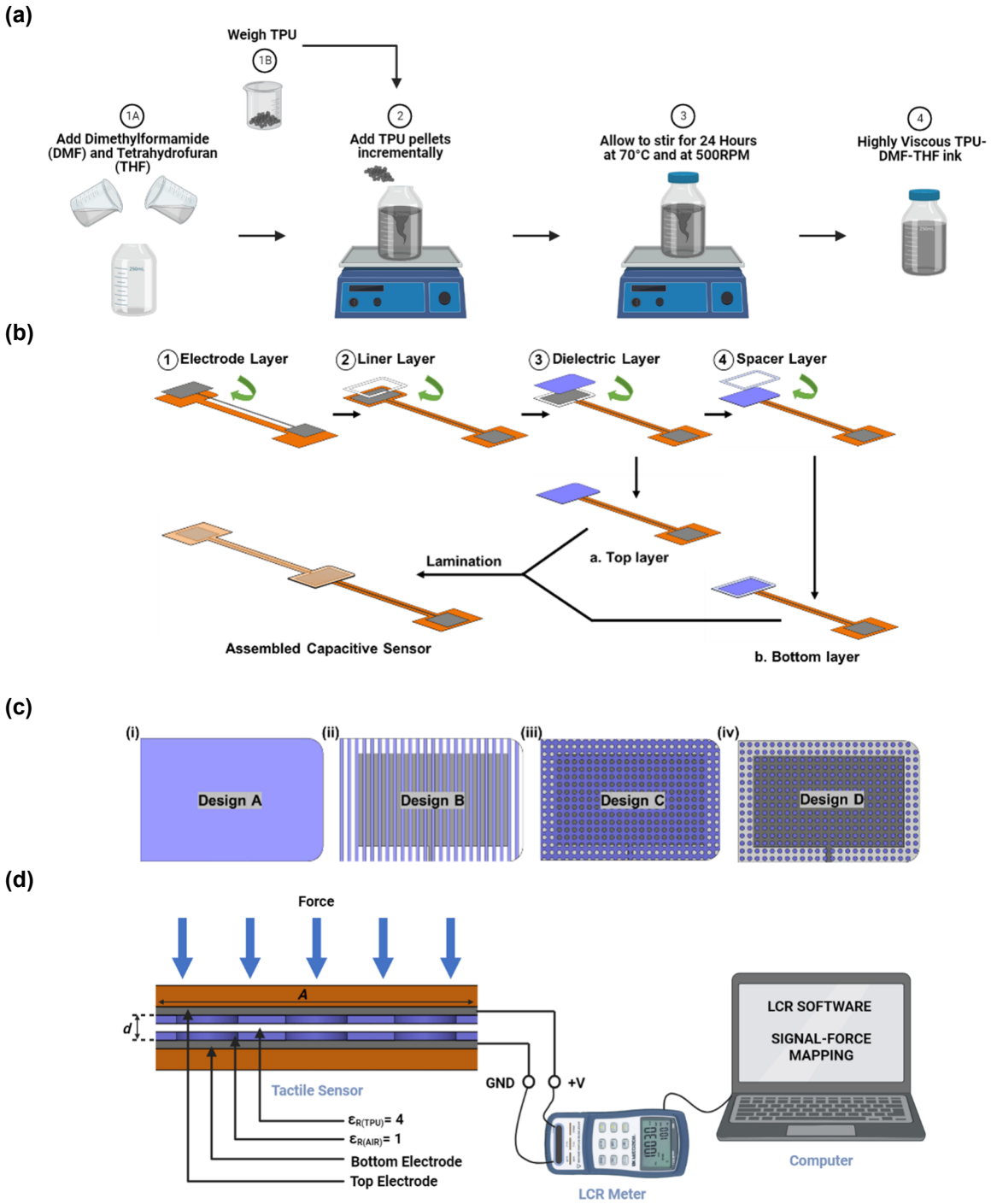

Figure 2. Schematic illustration for (a) fabrication process of TPU ink, (b) Screen printing fabrication process and assembly of capacitive tactile sensor, (c) CAD surface design of Dielectric layer for (i) Design A, ii) Design B, iii) Design C and iv) Design D, and (d) LCR Meter circuitry connection setup for Sensor-Computer Interface during characterization performance of capacitive tactile sensor.

2.3 Characterization

The viscosity behaviour of formulated TPU inks were characterized using an Anton Paar rheometer (MCR 702 MultiDrive). The measurements for the rheology characterization of the inks were performed at 25°C to

simulate screen printing at room temperature. The inks were subjected to increasing shear rates between 0.1-100 s^{-1} and the flowing material's viscosity behaviour was graphically represented through viscosity flow curves to verify shear thinning and the viscosity range for screen printing compatibility[17]. The viscoelastic behaviour of the inks was analyzed through amplitude sweeps to reflect dynamic conditions and determine the linear viscoelastic (LVE) range for liquid-like behaviour[17,18]. Furthermore, to simulate screen printing process, a time-dependent controlled-shear-rate test (step test) was performed. This included three intervals; measurement of viscosity at low shear rate to simulate the ink at rest, measurement of viscosity at high shear to simulate spreading the ink across the screen to fill the mesh opening and measurement of viscosity during structural recovery of the ink at low initial shear rate[18].

The analysis of the surface and cross-section morphologies of the screen-printed patterns of electrodes, liner, spacers, and micro-structured dielectric layers were performed using a scanning electron microscope (SEM – JSM-IT100, JEOL Corporation). To enhance charge transfer and for optimum SEM image quality, the screen-printed patterns were prepared with gold sputtering on the surface prior to observation through SEM[19]. Furthermore, the line width of the printed micro-structures was measured and observed using both an optical microscope (OMAX 40X-2000X, OMAX Microscope) and the SEM. The printed integrity of the conductive tracks and micro-structured dielectric were confirmed using the optical microscope in case of any ink bleeding or short circuits prior to sensor assembly. To further analyze the surface morphology, a surface roughness tester (Surftest SJ-210, Mitutoyo) was used to measure the surface roughness value (R_q, the root mean square of the profile values) of screen-printed patterns.

To check the base capacitance of assembled capacitive sensors, the electrodes through the conductive tracks were connected to an LCR Meter (B&K Precision 880 LCR Dual-Display Handheld Meter) as shown in Figure 2 (d). The capacitance of the capacitive tactile sensor was acquired in real-time at a frequency of 100 kHz in parallel mode with a maximum measurement rate of 4 sample readings per second via an LCR Software (B&K Precision) on a computer[20]. The capacitance signal readings were used to calculate the base capacitance of the four different capacitive tactile sensor designs without any pressure applied.

To evaluate the electromechanical performance of the assembled sensor designs, the sensors were subjected to compression tests using a universal tester (Instron 5848 Microtester) while the sensors' capacitance signals were acquired in real-time using the aforementioned Sensor-Computer interface. To mimic tool-tissue interaction during neurosurgeries with brain tissue (shore hardness 4.5 ± 1.5 Shore 00), a silicone rubber tip (EcoflexTM 00-10, Smooth-On Inc., East Texas, PA) of 24 mm^2 cross-section similar to dimensions of the gripper jaw surface area with shore hardness of 10 Shore 00 was fabricated and attached to the universal tester to apply perpendicular forces to the surface of the sensor[21,22]. Sensor performance and sensitivity of the four different capacitive tactile sensor designs from this setup were recorded, graphed, and analyzed for comparison.

Sensitivity (S) for the capacitive sensor was calculated as per the following equation:

$$S = \frac{\delta(\Delta C/C_0)}{\delta P} \quad (1)$$

$$\Delta C = C - C_0 \quad (2)$$

where C_0 is the base capacitance (initial capacitance without pressure), ΔC is the relative change of capacitance and P is the applied pressure on the sensor[23,24]. The pressures applied in this study are based on the forces applied on the interior gripper jaw of the surgical tool (24 mm^2). Force and pressure applied on the sensor are used interchangeably in this study due to the small surface area of the tactile sensor customized for the surface of the interior gripper jaw of the surgical tool.

3. Results and Discussion

3.1 Dielectric Ink Characterization

The purpose of the dielectric (insulator) ink characterization is to formulate a screen-printable TPU ink to print the dielectric layer, liner layer and spacer layer in the design of the proposed capacitive tactile sensor to separate the parallel superimposing electrode surfaces. The formulated tunable dielectric ink consists of two components; thermoplastic polyurethane as elastomer and dissolving solvents namely; DMF and THF. Pure

TPU was tuned to 10 wt%, 15 wt%, 20 wt%, 25 wt% and 30 wt% with DMF and THF solvents to determine optimum TPU ink constituents for the fabrication of TPU sub-layers and micro-structured TPU dielectric layers for the capacitive tactile sensor. Four rheological properties; high viscosity (approximately 1–100Pa·s for 1–10^3 s^{-1}), shear thinning (1-2.5 Pa·s at high shear rate), gel-like viscoelastic behaviour (G' > G''), and thixotropic behaviour (quick thixotropic recovery rate) of the TPU inks were tested to verify efficient and high quality deposition for optimum sensor sub-layer fabrication[17,25,26,27].

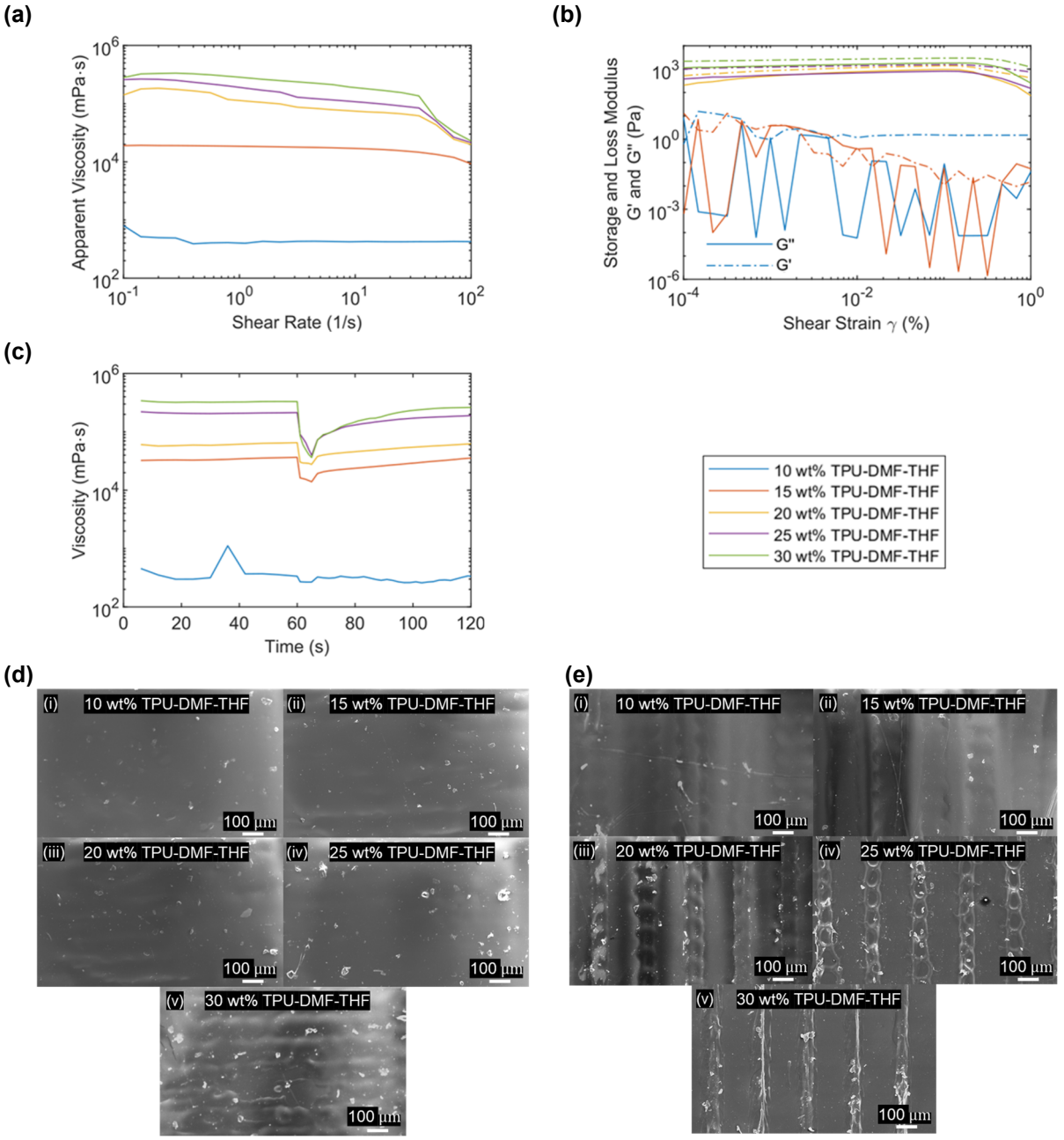

Figure 3. Rheology behaviour of TPU-DMF-THF ink (a) Flow curve, (b) Amplitude sweep, (c) Step Test, (d) Surface SEM of large screen-printed pattern (x100) for (i) 10 wt%, (ii) 15 wt%, (iii) 20 wt%, (iv) 25 wt%, and (v) 30 wt% TPU-DMF-THF, and (e) Surface SEM of screen-printed micro-structured pattern (x100) for (i) 10 wt%, (ii) 15 wt%, (iii) 20 wt%, (iv) 25 wt%, and (v) 30 wt% TPU-DMF-THF.

Rheological characterization results in Figure 3 (a), (b) and (c) indicated that 20 wt%, 25 wt% and 30 wt% TPU-DMF-THF ink solutions had high viscosity, a quick thixotropic recovery rate, high shear thinning and adequate gel-like viscoelastic behaviour. 10 wt% and 15 wt% TPU-DMF-THF ink solutions, on the other hand,

demonstrated low viscosity, low shear thinning and fluid viscoelastic behaviour (G'' > G') at certain shear strains[26]. As per Glasser et al., gel-like viscoelastic inks were preferred for ease of screen printing due to their high shear thinning property and gel-like viscoelastic behaviour (G' > G'') properties[26]. The results of the amplitude sweep in Figure 3 (b) show that 20 wt%, 25 wt% and 30 wt% TPU-DMF-THF ink demonstrated gel-like viscoelastic behaviour (G' > G''). Moreover, with increasing TPU content, storage modulus (G') subsequently increased making the ink more elastic and faster to regain its structure after deformation.

To verify the rheological results and to determine optimum TPU ink concentration for fabrication of TPU sub-layers and micro-structured TPU dielectric layers, the inks were screen printed using a 4 x 4 cm square pattern (large pattern) and a series of 100 µm line width pattern (micro-structured pattern) onto polyimide substrate. The large pattern was used to determine efficiency and quality of prints for the large printed surface while the micro-structured pattern was used to determine feasibility of printing 100 µm line width microfeatures for developing the four differing dielectric morphology designs. Figure 3 (d) shows the SEMs of the surface morphology of screen-printed TPU on the large surface for the different concentrations. Micropores and voids were identified for 25 wt% and 30 wt% TPU-DMF-THF prints from evaporation of the solvents when dried while 10 wt%, 15 wt% and 20 wt% TPU-DMF-THF ink produced adequate print quality with minimal traces of voids or micropores. The surface tension and mesh size also influence the resulting surface morphology with undulating shapes in Figure 3 (d) and (e) of the screen-printed TPU patterns. The measured thickness of the cross-section of screen-printed TPU layer for 100 µm line width for 10 wt%, 15 wt%, 20 wt%, 25 wt% and 30 wt% TPU-DMF-THF was 8.47 ± 2.60 µm, 9.16 ± 2.69 µm, 10.12 ± 2.43 µm, 10.75 ± 3.03 µm and 10.91= ± 3.54 µm respectively (n = 5 for each ink). The calculated wet thickness based on the screen printing mesh, as per the manufacturer, is 25 µm. The calculated dry thickness for screen-printed TPU layer for 10 wt%, 15 wt%, 20 wt%, 25 wt% and 30 wt% TPU-DMF-THF is 2.5 µm, 3.75 µm, 5 µm, 6.25 µm and 7.5 µm, respectively, if all the solvent evaporated. The surface SEM of screen-printed 100 µm line width pattern in Figure 3 (e) showed that 20 wt% TPU-DMF-THF ink produced the best quality of prints with minimal bleeding and a margin of error of 6.85% for the 100 µm line width pattern. The surface roughness (R_q) of screen-printed TPU for 100 µm line width for 10 wt%, 15 wt%, 20 wt%, 25 wt% and 30 wt% TPU-DMF-THF was 5.64 ± 2.49 µm, 5.87 ± 2.53 µm, 6.44 ± 2.48 µm, 7.42 ± 3.03 µm and 7.85 ± 4.47 µm respectively (n = 5 for each ink). Based on the print quality and the rheological characterization results, 20 wt% TPU-DMF-THF ink was chosen for screen printing the micro-structured dielectric layer, liner layer and spacer layer for the proposed capacitive tactile sensor.

3.2 Dielectric Layer Design Optimization

To improve the sensitivity and performance of the proposed capacitive tactile sensor, four dielectric layer designs were developed with varying surface morphologies as shown in Figure 2 (c) and then screen printed onto screen-printed electrode substrates. Each design involved a different surface area of TPU which impacted the structural properties of the dielectric layer and in turn affected the change in capacitance during compression of the overall sensor[16,28]. The four developed dielectric layer designs consisted of Design A, B, C and D with TPU microstructures of surface areas of 15 mm^2, 6 mm^2, 8.33 mm^2 and 4.24 mm^2 respectively. Figure 4 (a) depict the SEM of the surface morphology of printed dielectric layer designs on screen-printed electrode substrates.

The top layer and bottom layer with corresponding dielectric layer designs (Design A, B, C and D) were assembled as outlined in Figure 2 (b) and 5 sensors for each design were fabricated. The base capacitance, C_0, of each fabricated sensor was verified to ensure adequate construction and lamination. The measured base capacitance, C_0, of the assembled capacitive tactile sensors for Design A, B, C and D averaged 9.48 ± 0.63 pF, 7.77 ± 0.61 pF, 8.41 ± 0.43 pF and 7.36 ± 0.44 pF, respectively (n = 5 for each design) (See Supporting Information, Table S1 for base capacitance for each dielectric layer design). A margin of error of 7.6%, 12.1%, 11.5% and 15.9% was obtained when comparing the measured base capacitance with the calculated values for Designs A, B, C, and D, respectively. The calculated base capacitance values of 8.81 pF, 6.93 pF, 7.54 pF and 6.35 pF for Design A, B, C and D, respectively, were determined using the area of overlapping parallel facing electrodes (A = 15 mm^2) and separation thickness (d) of the series mix of dielectric mediums (air gap, $\varepsilon_{r,air}$=1, and 2 dielectric TPU layers, $\varepsilon_{r,TPU}$=4, at total thickness, d, of 30 µm for each design) (See Supporting Information for Base Capacitance Calculation). The margin of error between

measured and calculated base capacitance for the fabricated sensors can be associated with assembly and fabrication errors.

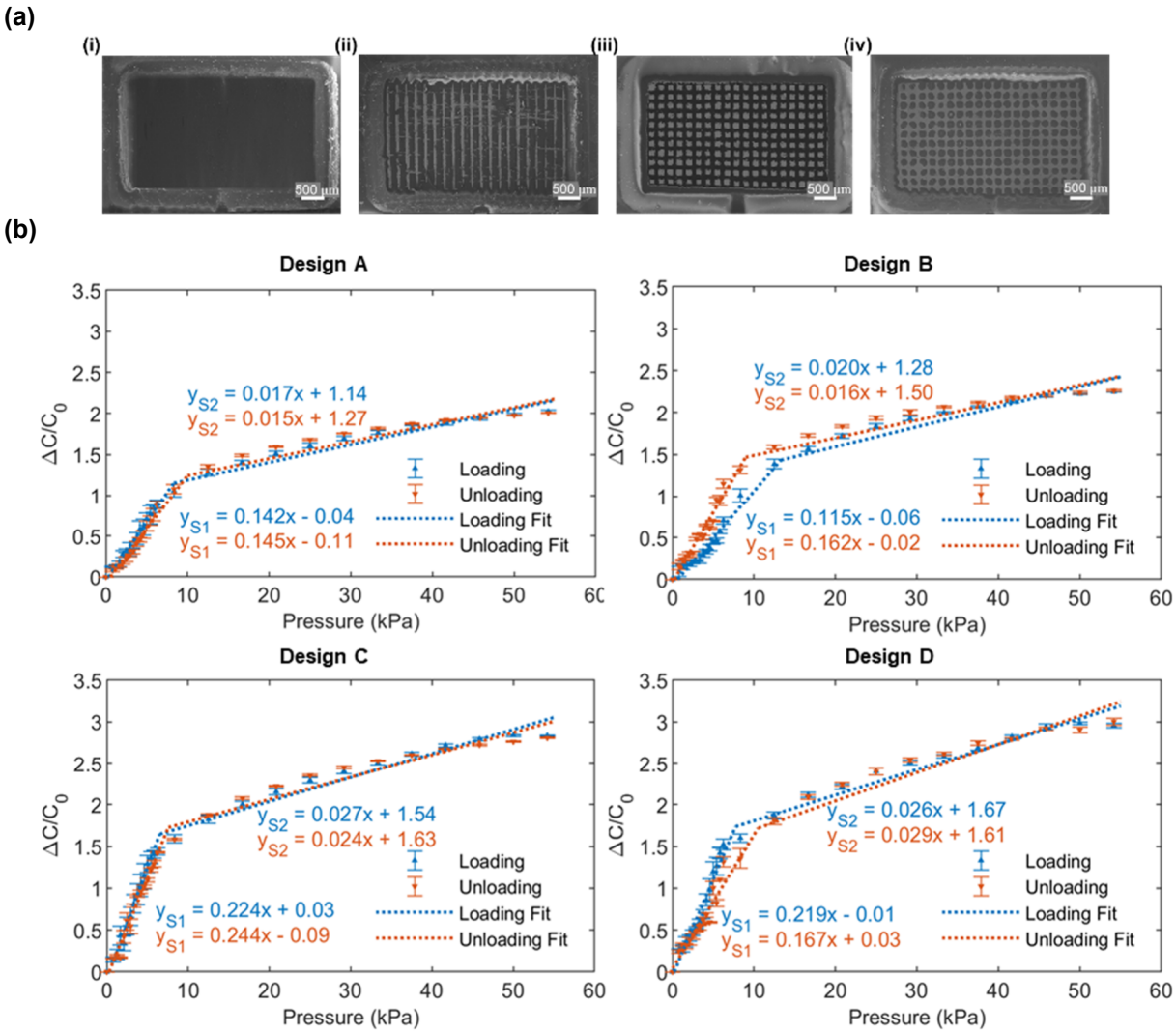

Figure 4. (a) SEM of surface of screen-printed 20 wt% TPU dielectric on electrode with liner x15 for (i) Design A, ii) Design B, iii) Design C and iv) Design D, (b) Characterization of dielectric layer and performance of 5 fabricated sensors with different TPU dielectric morphologies for Design A, Design B, Design C and Design D (*n* = 5, error bars denote s.d.).

To investigate the effect of dielectric morphology on sensor performance, 5 fabricated sensors for each design were subjected to compressive loadings while the capacitance was acquired in real-time using the sensor-computer interface with the LCR meter. Figure 4 (b) shows the capacitance change due to the influence of compressive loads on the assembled capacitive sensors for Designs A, B, C and D (See Supporting Information, Figure S1 for average performance for sensors for Designs A, B, C and D). Based on the response, two distinct linear pressure ranges with corresponding sensitivities were identified for all four variations of the sensor. The sensitivities of the sensors were determined by the slope of the linear fits on the curve (relative change of capacitance with change in applied pressure). Based on literature, microstructures in the design of elastomer dielectrics can affect the deformation of the dielectric layer thereby affecting the separation between the electrodes (*d*) and capacitance during compression[16]. In this study, microstructures in the design of the dielectric were observed to increase the relative change of capacitance which can be rationale by an ease and increase in deformation of the dielectric (decrease in *d*). Furthermore, a decrease in hysteresis and improved sensitivities (in low pressure range) was associated with the dielectric layers with microstructures. Non-patterned dielectric design (Design A) had the smallest relative change of

capacitance upon compression while Designs B and D exhibited more hysteresis, noisy responses, and low sensitivities. Hence, with a high relative change of capacitance (0 – 2.8), minimal hysteresis and high sensitivities for loading and unloading, Design C with surface area of 8.33 mm^2 was chosen as the best candidate for the dielectric layer design of the capacitive tactile sensor.

3.3 Assembled Sensor Fabrication and Working Mechanism

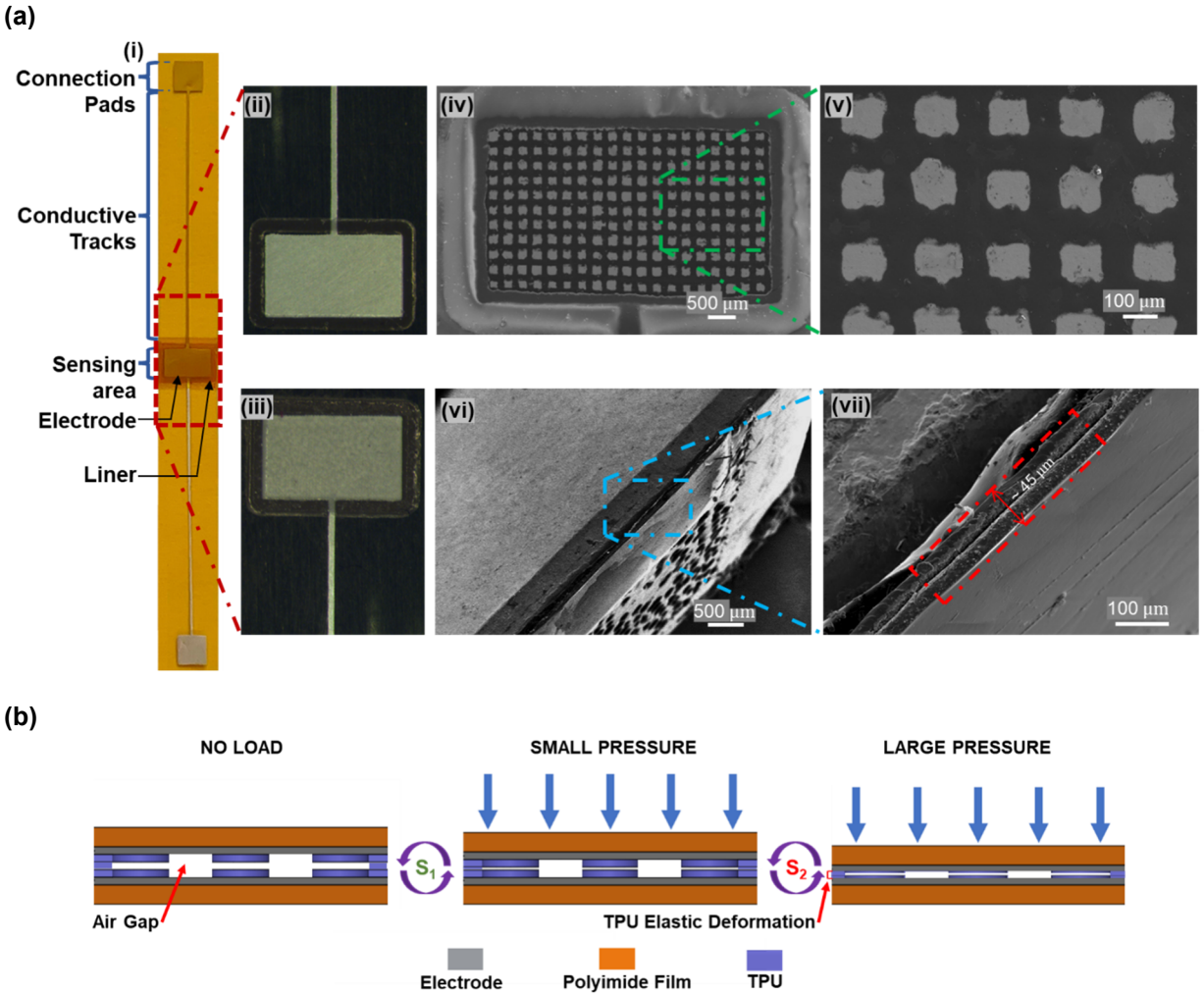

Figure 5. (a) Characteristics of printed film (i) Photograph image of capacitive tactile sensor printed on polyimide substrate, (ii) Optical microscopic image of surface of screen-printed electrode with liner x4, (iii) Optical microscopic image of surface of screen-printed Bottom layer (electrode with liner, Dielectric Design C and spacer layer) x4, (iv) SEM of surface of Top layer x15, (v) SEM of surface of Top layer (screen-printed 20 wt% TPU) x100, (vi) SEM of cross-section of Top layer x25, (vii) SEM of cross-section of Top layer x150, (b) Schematic illustration of capacitive transduction method and working mechanism of capacitive tactile sensor.

The proposed capacitive tactile sensor used dielectric Design C in the multilayered sensor design. The average base capacitance for the proposed sensor with dielectric Design C was 8.41 ± 0.43 pF (n = 5). The multiple layers were screen-printed in chronological order, and then the top layer and bottom layer were superimposed, laminated, and sealed as shown in Figure 5 (a) (i). Figure 5 (a) (iv) and (v) shows the SEM of the surface morphology of screen-printed top layer with dielectric Design C prior to assembly. The SEM image shows a grid-like micro-structured TPU layer with spacing and line width of 95.13 ± 11.16 µm (n = 10). For 100 µm line width of screen-printed electrode layer ((n = 5), the calculated wet thickness of the screen-printed silver electrode was 25 µm, the measured thickness was 10.36 ± 0.63 µm and the measured surface roughness, R_q, was 3.51 ± 0.63 µm. The geometric dimensions of the assembled sensor involved a sensing

area of 15 mm^2 (A) with 0.5 mm clearance and an overall thickness of 100 ± 3 µm (n = 10) µm to meet the physical requirements for attachment to the 24 mm^2 surface area of the interior jaw of the magnetically-controlled microgripper to adequately monitor grasping forces during endoscopic intraventricular surgeries. In comparison with previous reports on screen-printed capacitive pressure sensors in Table 2, it is seen that the geometry, thickness and size of existing sensors are not suitable for attachment to the interior jaw of the magnetically-controlled microgripper.

The working mechanism of the capacitive tactile sensor can be divided into two modes; firstly, structural deformation of the top layer into the air gap, S_1, and secondly elastic deformation of the TPU dielectric layer, S_2, as shown in Figure 5 (b). For S_1, when small pressures are applied, the structure of the top layer—which includes the polyimide, top electrode, and dielectric layer—deforms into the air gap between the top and bottom dielectric layers. This deformation compresses the air dielectric medium, reducing the separation between the electrodes. Since air is a compressible medium, it absorbs the deformation by decreasing in volume without being displaced and without affecting the seal's integrity. Upon loading with large pressures for S_2, the grid-like TPU microstructures undergo elastic deformation, compressing into the spacing between them and reducing the overall thickness (d) of the TPU dielectric medium. This compression continues to decrease the distance between the electrodes, further increasing the capacitance. During unloading for S_2, the grid-like TPU layer regains its initial shape, thereby increasing the thickness (d) of the dielectric medium between the electrodes. When small pressures are removed (S_1), the compressed air within the dielectric gap decompresses and returns to its original volume. The TPU liner facilitates this decompression by acting as a cushion, ensuring the air gap regains its initial shape without causing mechanical stress to the overall structure. Overall, the deformation due to applied pressure on the sensor changes the thickness (d) of the series of dielectric medium within the sensor assembly which in turn, varies the capacitance signal acquired in real-time.

3.4 Sensor Electromechanical Performance

To characterize the proposed assembled capacitive sensor, the Sensor-Computer interface with the LCR meter was connected to the sensor while subjecting it to cyclic compression tests using a universal tester for 10 fabricated sensors (n = 10). The characterization is depicted in Figure 6 and Figure 7. The assembled capacitive sensors with dielectric Design C's sensor performance are summarized in Table 1 and compared with existing screen-printed capacitive sensors in Table 2.

A. Range and Time Response

To determine the minimum pressure detectable by the sensors (n = 10), the ratio of relative change of capacitance to initial capacitance was calculated based on the acquired capacitance signal at a loading frequency of 2.71 kPa/s. This signal was then superimposed with the stimuli reference pressure signal, using the signals' timestamps as reference points, shown in Figure 6 (a) and (b). Based on the graph, the sudden rise in capacitance signal was used to determine the minimum detectable pressure. Through multiple tests for each sensor, the average minimum detectable pressure was 0.44 ± 0.2 kPa at 4 s. To determine the working range of the sensor, the relative capacitance to initial capacitance ratio was mapped against the stimuli reference pressure to establish a capacitance signal-pressure relationship as shown in Figure 6 (c). Based on the working mechanism of the sensor and the signal pressure mapping, two distinct working ranges; low pressure range (S_1) and large pressure range (S_2) were identified. S_1 ranged between 0.42 – 6.25 kPa and S_2 ranged between 6.25 – 54.2 kPa. The sensor detected a maximum peak signal at 54.2 kPa.

Based on the signal-pressure mapping (Figure 6 (c)), a working range of 0.42 – 54.2 kPa (0.01 - 1.30 N applied on 24 mm^2 of gripper jaw) was determined to be apt for minimally invasive endoscopic intraventricular surgeries. This range is suitable because it overlaps with the force range associated with brain injury, which is between 0.49 - 0.88 N, and 70% of surgical tasks in neurosurgery require forces of less than 0.3 N[10,29]. Furthermore, based on the design requirements of the microgripper, grasping forces up to 0.181 N (7.54 kPa) was targeted for microneurosurgical procedures which is well within the pressure/force range of the proposed capacitive sensor for monitoring grasping performances[2,5]. Using Figure 6 (a), the delay, t, between the peaks of the reference pressure and the acquired capacitance signal were compared to determine the sensor time response and a calculated value of 110 ± 40 ms was obtained, which is within the unnoticed time delay (200

ms) by surgeons as per literature and is superior to current screen-printed capacitive pressure sensors, as shown in Table 2[30].

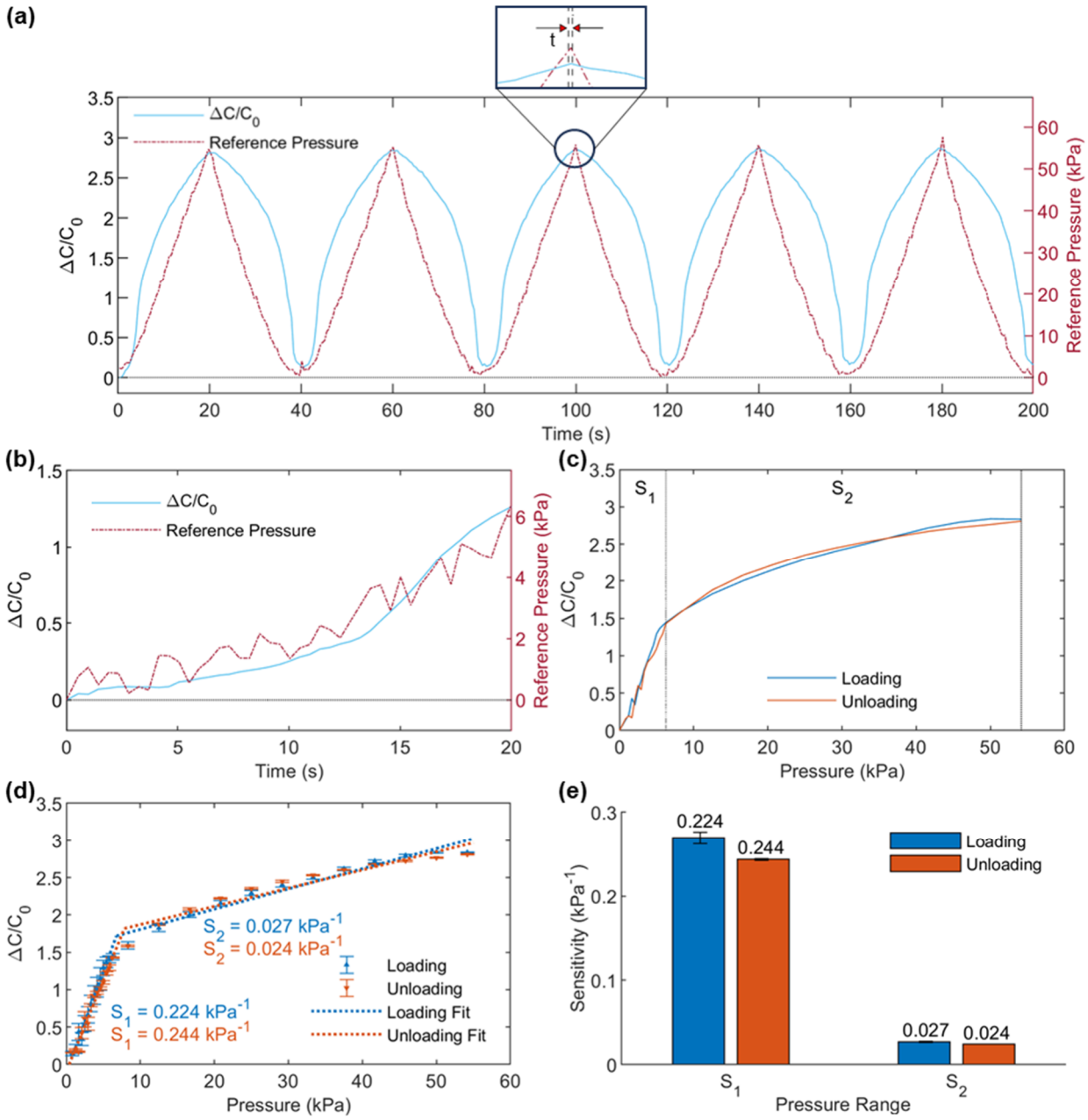

Figure 6. (a) Capacitive tactile sensor response to cyclic compression loading at frequency of 2.71 kPa/s for pressure range of 0 - 54.2 kPa (*n* = 10), (b) Response of Capacitive tactile sensor for small pressure ranges (*n* = 10), (c) Sensor signal-pressure relationship between 0 and 54.2 kPa for loading and unloading (*n* = 10), (d) Bi-linear modelling of sensor signal-pressure relationship between 0 and 54.2 kPa for loading and unloading for S_1 and S_2 (*n* = 10, error bars denote s.d.), (e) Sensitivities for small and large pressure ranges for loading and unloading of the proposed capacitive tactile sensor (*n* = 10, error bars denote s.d.).

B. Sensitivity and Hysteresis

To analyze the characteristics of the working ranges of the sensor, linear fitting curves as shown in Figure 6 (d) were used to model the signal-pressure relationship for S_1 and S_2 for both loading and unloading. The linearity of the models was ensured by maintaining correlation coefficient R^2 values greater than 0.90. Using the slope of the linear fit, the sensitivities for loading and unloading for low pressure ranges, S_1, were determined as 0.224 ± 0.007 kPa^{-1} and 0.244 ± 0.001 kPa^{-1} respectively. A paired t-test was used to compare

the mean loading and unloading sensitivities to determine whether there is a statistically significant difference between them. Based on a 95% confidence interval, the sensitivity difference for loading and unloading for S_1 were insignificant ($p = 0.13 > 0.05$). For large pressure ranges, S_2, based on the linear fittings, the sensitivities for loading and unloading were 0.0270 ± 0.0008 kPa^{-1} and 0.0240 ± 0.0002 kPa^{-1} respectively. The sensitivity difference for S_2 for loading and unloading is significant based on a 95% confidence interval ($p = 0.005 < 0.05$).

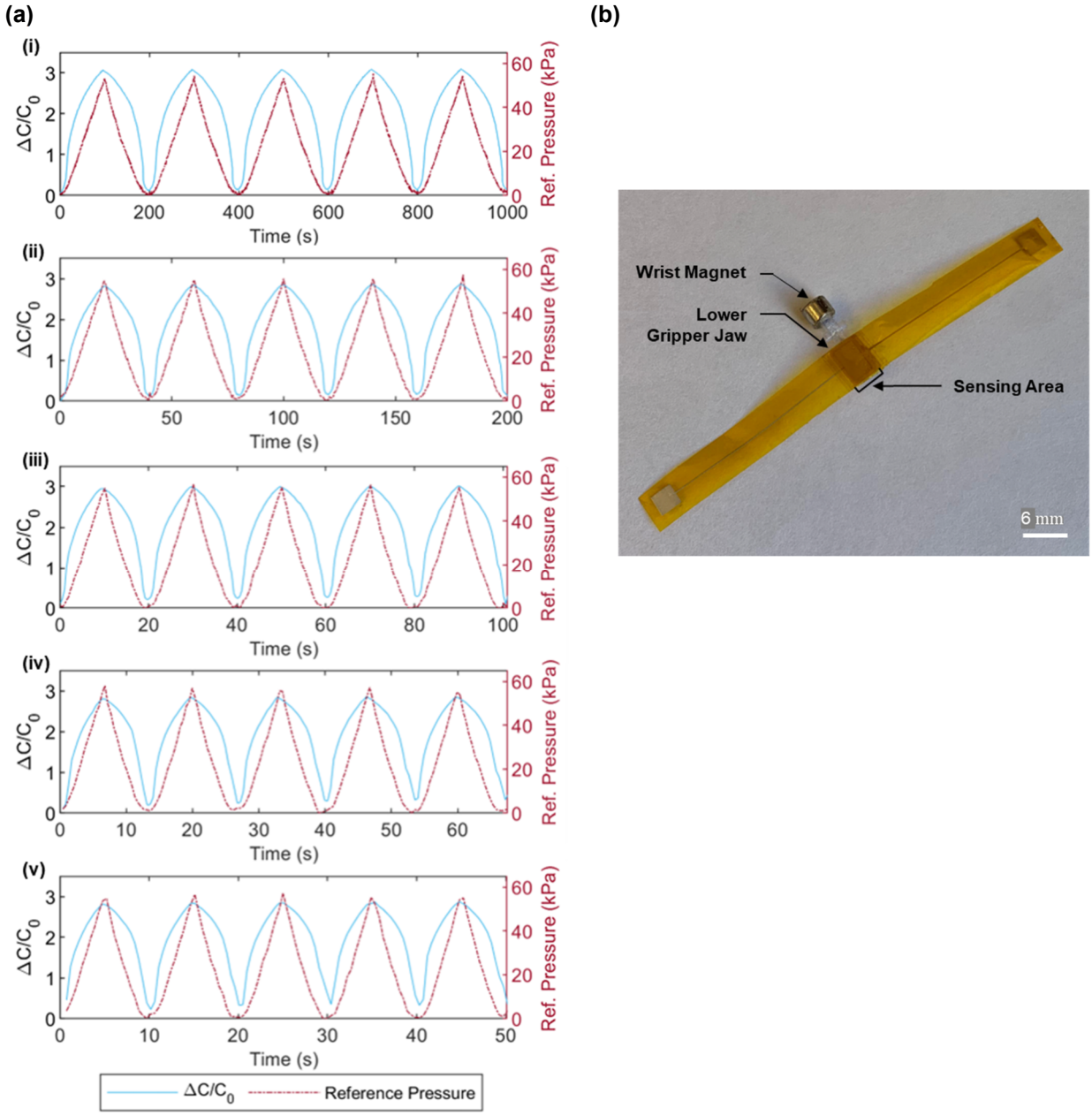

Figure 7. (a) Measured sensor response and reference pressure under different loading frequencies (i) 0.54 kPa/s, (ii) 2.71 kPa/s, (iii) 5.42 kPa/s, (iv) 8.33 kPa/s and (v) 10.8 kPa/s (n = 10), and (b) Photograph of assembled Capacitive Tactile Sensor with Dielectric Design C layer attached to lower jaw of Microgripper.

Figure 6 (e) outlines the difference between the two linear ranges and their respective loading and unloading sensitivities. With increasing pressure, there is, therefore, a significant decrease in sensitivity during the transition between the small pressure range and large pressure range. These sensitivities are comparable to existing screen-printed capacitive pressure sensors of similar sizes, as shown in Table 2. The maximum hysteresis was observed to occur in the working range of S_1 at 1.7 kPa with the largest signal deviation

between loading and unloading with an error value of ± 8.8%. Overall, the capacitive sensor experienced low hysteresis (< 10%) which ensures quality of tactile feedback for monitoring tool-tissue manipulation during minimally invasive endoscopic intraventricular surgeries[29].

C. Resolution and Repeatability

To determine resolution, a sample size of 10 capacitive tactile sensors were analyzed. Using Figure 6 (b), the smallest pressure required to create a change in the ratio of relative change of capacitance to initial capacitance by 0.01 was an average resolution of 0.58 kPa. This is relatively high and could stem from equipment limitations and a low sampling rate. For repeatability and to verify performance for multiple loading and unloading cycles during surgery, the tactile sensor was subjected to 5 cyclic loadings at high and low pressures for frequencies 0.54 kPa/s, 2.71 kPa/s, 5.42 kPa/s, 8.33 kPa/s and 10.8 kPa/s. The relative capacitance change was superimposed against the reference stimuli pressure for each frequency as shown in Figure 7 (a). The results indicated no significant changes in capacitance for increasing frequencies for the same loading based on the peak low and high signals. The tactile sensor demonstrated considerable stabilities over 5 cycles with an average decay between peaks of 0.48%, 1.78% 1.85%, 1.57% and 1.30% for frequencies of 0.54 kPa/s, 2.71 kPa/s, 5.42 kPa/s, 8.33 kPa/s and 10.8 kPa/s respectively. With a decay of less than 5%, the sensor indicates good sensor stability performance to be potentially used in RMIS application. Furthermore, the sensed pressure indicated no declination with increasing loading frequencies.

Table 1: Summary of Capacitive Tactile Sensor Performance after Optimization (n = 10)

Description	Value
Minimum Detectable Pressure	0.44 ± 0.2 kPa
Time Response	110 ± 40 ms
Sensitivity S_1: 0.42 – 6.25 kPa (Loading) 0.42 – 6.25 kPa (Unloading) S_2 6.25 – 54.2 kPa (Loading) 6.25 – 54.2 kPa (Unloading)	 0.224 ± 0.007 kPa^{-1} 0.244 ± 0.001 kPa^{-1} 0.0270 ± 0.0008 kPa^{-1} 0.0240 ± 0.0002 kPa^{-1}
Sensitivity Difference	S_1: p = 0.13 > 0.05 (Not Significant) S_2: p = 0.005 < 0.05 (Significant)
Resolution	0.58 kPa
Range	S_1: 0.42 – 6.25 kPa S_2: 6.25 – 54.2 kPa
Hysteresis	At 1.7 kPa (8.8%)

Table 2. A summary of the reported performance of existing screen-printed and partially screen-printed capacitive pressure sensors.

Dielectric material	Electrode material	Thickness [µm]	Geometry	Sensing Area [mm^2]	Operating pressure range [kPa]	Loading Sensitivity [kPa^{-1}]	Response time [ms]	Ref.
PDMS	Ag	200	Rectangle	200	800–1.8 × 10^4	-	-	[31]
PDMS	Ag	48.2	Square	144	200–2400	-	-	[32]
P(VDF–TrFE)	Ag	139	Square	1	$3.3×10^4$–$5.5×10^4$	-	-	[33]
CNTs/ PDMS	Ag	-	Square	100	0-$450×10^{-3}$ $450×10^{-3}$-$850×10^{-3}$	2.9 1.87	-	[34]
Air/Ecoflex-0030	PEDOT:PS	2800	Square	3600	−60 to 20	0.34		[35]
Parylene C	Ag	-	Square	144	0.07–1.39	0.124	580 ± 50	[36]
Air/TPU	Ag	100	Rectangle	15	0.44–625 6.25 – 54.2	0.224 0.0270	110 ± 40	This work

4. Conclusion

This work demonstrated that screen printing technology could be used in place of photolithography and chemical etching to fabricate high performance capacitive tactile sensors to be mounted onto unique interior gripper surfaces of millimeter-scale surgical tools used in RMIS to potentially improve grasping performances and quality of endoscopic intraventricular surgeries. To demonstrate this, in this study, the capacitive sensor was customized for the interior jaws of a 4 mm diameter surgical tool prototype as shown in Figure 7 (b) to remedy size (scale), sensibility and sensitivity limitations unique to endoscopic intraventricular surgeries[5].

For future work, the proposed sensor could be attached to the interior jaw of the microgripper wirelessly with inductive coupling within the inner groove of the microgripper tool. Alternatively, the conductive tracks and connection pads could be designed to pass through the inner groove of the tool (groove shown in Figure 1 (b)). These designs would avoid impacting the base capacitance and prevent any interference with the grasping or navigation of the surgical tool during RMIS. To further decrease the thickness of the tactile sensor and avoid impeding grasping performance, the sublayers of the capacitive tactile sensor could be directly printed onto the smooth, flat, and rigid surface of the interior of the 3D-printed microgripper jaws. These sublayers could then be coated with a biocompatible polymer composite that provides shielding against electromagnetic interference. This might also eliminate attachment hurdles when mounting the sensors onto the tool. Data acquisition equipment with a higher sampling rate could be used to acquire tactile information in real-time and to verify resolution and repeatability more accurately. To characterize the sensor further, the sensitivity models for each pressure range could be used to map tactile pressures subjected to the sensor. The tactile feedback could be used to verify accuracy of the model and the sensor against the stimuli reference pressure. Next steps for the capacitive tactile sensor's development would involve calibration and optimization for clinical application (ex-vivo, in-vivo, and cadaver studies) to test sensor performance and quality of tactile feedback. The findings in this study can be expected to improve performance, quality, and safety of endoscopic intraventricular surgeries and RMIS.

5. Supporting Information

Supporting Information: Average performance of capacitive tactile sensors with different TPU dielectric morphologies; detailed calculation of base capacitance of capacitive tactile sensors; base capacitance analysis of fabricated capacitive sensors; additional figures (PDF)

6. Author Information

Corresponding Author

Hani E. Naguib − Department of Mechanical and Industrial Engineering, University of Toronto, Toronto, Ontario M5S 3G8, Canada; Institute of Biomedical Engineering, University of Toronto, Toronto, Ontario M5S 3G9, Canada; Toronto Rehabilitation Institute, Toronto, Ontario M5G 2A2, Canada; orcid.org/0000-0003-4822-9990; Email: naguib@mie.utoronto.ca

Authors

D. Anastasia Aubeeluck − Department of Mechanical and Industrial Engineering, University of Toronto, Toronto, Ontario M5S 3G8, Canada

Cameron Forbrigger − Department of Mechanical and Industrial Engineering, University of Toronto, Toronto, Ontario M5S 3G8, Canada

Sara Mohseni Taromsari − Department of Mechanical and Industrial Engineering, University of Toronto, Toronto, Ontario M5S 3G8, Canada

Tianhao Chen − Institute of Biomedical Engineering, University of Toronto, Toronto, Ontario M5S 3G9, Canada

Eric Diller − Department of Mechanical and Industrial Engineering, University of Toronto, Toronto, Ontario M5S 3G8, Canada; University of Toronto Robotics Institute, University of Toronto Engineering, Toronto, Ontario M5S 1A4, Canada

Notes

The authors declare no competing financial interest.

7. Acknowledgements

The authors would like to thank the financial support from the Canadian Institutes of Health Research (CIHR) and the Natural Science and Engineering Research Council of Canada (NSERC).

8. References

(1) van Assenbergh, P.; Culmone, C.; Breedveld, P.; Dodou, D. Implementation of Anisotropic Soft Pads in a Surgical Gripper for Secure and Gentle Grip on Vulnerable Tissues. *Proc Inst Mech Eng H* 2021, *235* (3), 255–263. https://doi.org/10.1177/0954411920971400.

(2) Forbrigger, C.; Lim, A.; Onaizah, O.; Salmanipour, S.; Looi, T.; Drake, J.; Diller, E. D. Cable-Less, Magnetically Driven Forceps for Minimally Invasive Surgery. *IEEE Robot Autom Lett* 2019, *4* (2), 1202–1207. https://doi.org/10.1109/LRA.2019.2894504.

(3) Trejos, A. L.; Patel, R. V.; Naish, M. D.; Lyle, A. C.; Schlachta, C. M. A Sensorized Instrument for Skills Assessment and Training in Minimally Invasive Surgery. *J Med Device* 2009, *3* (4). https://doi.org/10.1115/1.4000421.

(4) Baki, P.; Szekely, G.; Kosa, G. Miniature Tri-Axial Force Sensor for Feedback in Minimally Invasive Surgery. In *2012 4th IEEE RAS & EMBS International Conference on Biomedical Robotics and Biomechatronics (BioRob)*; IEEE, 2012; pp 805–810. https://doi.org/10.1109/BioRob.2012.6290770.

(5) Forbrigger, C.; Fredin, E.; Diller, E. Evaluating the Feasibility of Magnetic Tools for the Minimum Dynamic Requirements of Microneurosurgery. In *2023 IEEE International Conference on Robotics and Automation (ICRA)*; IEEE, 2023; pp 4703–4709. https://doi.org/10.1109/ICRA48891.2023.10160840.

(6) Lim, A.; Schonewille, A.; Forbrigger, C.; Looi, T.; Drake, J.; Diller, E. Design and Comparison of Magnetically-Actuated Dexterous Forceps Instruments for Neuroendoscopy. *IEEE Trans Biomed Eng* 2021, *68* (3), 846–856. https://doi.org/10.1109/TBME.2020.3007581.

(7) George B, L.; Bharanidaran, R. Design of Compliant Gripper for Surgical Applications. *Australian Journal of Mechanical Engineering* 2022, *20* (1), 256–262. https://doi.org/10.1080/14484846.2019.1701396.

(8) Tiwana, M. I.; Redmond, S. J.; Lovell, N. H. A Review of Tactile Sensing Technologies with Applications in Biomedical Engineering. *Sens Actuators A Phys* 2012, *179*, 17–31. https://doi.org/10.1016/j.sna.2012.02.051.

(9) Chi, C.; Sun, X.; Xue, N.; Li, T.; Liu, C. Recent Progress in Technologies for Tactile Sensors. *Sensors* 2018, *18* (4), 948. https://doi.org/10.3390/s18040948.

(10) Gan, L. S.; Zareinia, K.; Lama, S.; Maddahi, Y.; Yang, F. W.; Sutherland, G. R. Quantification of Forces During a Neurosurgical Procedure: A Pilot Study. *World Neurosurg* 2015, *84* (2), 537–548. https://doi.org/10.1016/j.wneu.2015.04.001.

(11) Kim, J.; Kumar, R.; Bandodkar, A. J.; Wang, J. Advanced Materials for Printed Wearable Electrochemical Devices: A Review. *Adv Electron Mater* 2017, *3* (1). https://doi.org/10.1002/aelm.201600260.

(12) Gao, L.; Zhu, C.; Li, L.; Zhang, C.; Liu, J.; Yu, H.-D.; Huang, W. All Paper-Based Flexible and Wearable Piezoresistive Pressure Sensor. *ACS Appl Mater Interfaces* 2019, *11* (28), 25034–25042. https://doi.org/10.1021/acsami.9b07465.

(13) Zhang, Y.; Zhu, Y.; Zheng, S.; Zhang, L.; Shi, X.; He, J.; Chou, X.; Wu, Z.-S. Ink Formulation, Scalable Applications and Challenging Perspectives of Screen Printing for Emerging Printed Microelectronics. *Journal of Energy Chemistry* 2021, *63*, 498–513. https://doi.org/10.1016/j.jechem.2021.08.011.

(14) Pourghodrat, A.; Nelson, C. A. Disposable Fluidic Actuators for Miniature In-Vivo Surgical Robotics. *J Med Device* 2017, *11* (1). https://doi.org/10.1115/1.4035005.

(15) Cao, S.; Li, R.; Panahi-Sarmad, M.; Chen, T.; Xiao, X. A Flexible and Highly Sensitive Capacitive Pressure Sensor With Microstructured Dielectric TPU Layer Based on Mesh Fabric as Template. *IEEE Sens J* 2022, *22* (21), 20276–20284. https://doi.org/10.1109/JSEN.2022.3207005.

(16) Li, R.; Zhou, Q.; Bi, Y.; Cao, S.; Xia, X.; Yang, A.; Li, S.; Xiao, X. Research Progress of Flexible Capacitive Pressure Sensor for Sensitivity Enhancement Approaches. *Sens Actuators A Phys* 2021, *321*, 112425. https://doi.org/10.1016/j.sna.2020.112425.

(17) Lin, H.-W.; Chang, C.-P.; Hwu, W.-H.; Ger, M.-D. The Rheological Behaviors of Screen-Printing Pastes. *J Mater Process Technol* 2008, *197* (1–3), 284–291. https://doi.org/10.1016/j.jmatprotec.2007.06.067.

(18) Gao, Y.; Feng, J.; Liu, F.; Liu, Z. Effects of Organic Vehicle on the Rheological and Screen-Printing Characteristics of Silver Paste for LTCC Thick Film Electrodes. *Materials* 2022, *15* (5), 1953. https://doi.org/10.3390/ma15051953.

(19) Novikov, I. V.; Krasnikov, D. V.; Vorobei, A. M.; Zuev, Y. I.; Butt, H. A.; Fedorov, F. S.; Gusev, S. A.; Safonov, A. A.; Shulga, E. V.; Konev, S. D.; Sergeichev, I. V.; Zhukov, S. S.; Kallio, T.; Gorshunov, B. P.; Parenago, O. O.; Nasibulin, A. G. Multifunctional Elastic Nanocomposites with Extremely Low Concentrations of Single-Walled Carbon Nanotubes. *ACS Appl Mater Interfaces* 2022, *14* (16), 18866–18876. https://doi.org/10.1021/acsami.2c01086.

(20) B. P. Corporation. *Model 880 - Datasheet*. https://www.bkprecision.com/products/component-testers/880 (accessed Jan 21, 2023)

(21) Navarro-Lozoya, M.; Kennedy, M. S.; Dean, D.; Rodriguez-Devora, J. I. Development of Phantom Material That Resembles Compression Properties of Human Brain Tissue for Training Models. *Materialia (Oxf)* 2019, *8*, 100438. https://doi.org/10.1016/j.mtla.2019.100438.

(22) Aubeeluck, D. A.; Forbrigger, C.; Taromsari, S. M.; Chen, T.; Diller, E.; Naguib, H. E. Screen-Printed Resistive Tactile Sensor for Monitoring Tissue Interaction Forces on a Surgical Magnetic Microgripper. *ACS Appl Mater Interfaces* 2023, *15* (28), 34008–34022. https://doi.org/10.1021/acsami.3c04821.

(23) Ji, B.; Zhou, Q.; Lei, M.; Ding, S.; Song, Q.; Gao, Y.; Li, S.; Xu, Y.; Zhou, Y.; Zhou, B. Gradient Architecture-Enabled Capacitive Tactile Sensor with High Sensitivity and Ultrabroad Linearity Range. *Small* 2021, *17* (43). https://doi.org/10.1002/smll.202103312.

(24) Wan, Y.; Qiu, Z.; Hong, Y.; Wang, Y.; Zhang, J.; Liu, Q.; Wu, Z.; Guo, C. F. A Highly Sensitive Flexible Capacitive Tactile Sensor with Sparse and High-Aspect-Ratio Microstructures. *Adv Electron Mater* 2018, *4* (4). https://doi.org/10.1002/aelm.201700586.

(25) Donley, G. J.; Hyde, W. W.; Rogers, S. A.; Nettesheim, F. Yielding and Recovery of Conductive Pastes for Screen Printing. *Rheol Acta* 2019, *58* (6–7), 361–382. https://doi.org/10.1007/s00397-019-01148-w.

(26) Glasser, A.; Cloutet, É.; Hadziioannou, G.; Kellay, H. Tuning the Rheology of Conducting Polymer Inks for Various Deposition Processes. *Chemistry of Materials* 2019, *31* (17), 6936–6944. https://doi.org/10.1021/acs.chemmater.9b01387.

(27) Phair, J. W.; Lundberg, M.; Kaiser, A. Leveling and Thixotropic Characteristics of Concentrated Zirconia Inks for Screen-Printing. *Rheol Acta* 2009, *48* (2), 121–133. https://doi.org/10.1007/s00397-008-0301-4.

(28) Yoon, J. Il; Choi, K. S.; Chang, S. P. A Novel Means of Fabricating Microporous Structures for the Dielectric Layers of Capacitive Pressure Sensor. *Microelectron Eng* 2017, *179*, 60–66. https://doi.org/10.1016/j.mee.2017.04.028.

(29) Marcus, H. J.; Zareinia, K.; Gan, L. S.; Yang, F. W.; Lama, S.; Yang, G.; Sutherland, G. R. Forces Exerted during Microneurosurgery: A Cadaver Study. *The International Journal of Medical Robotics and Computer Assisted Surgery* 2014, *10* (2), 251–256. https://doi.org/10.1002/rcs.1568.

(30) Ladoiye, J. S.; Necsulescu, D. S.; Sasiadek, J., Control of Force in Surgical Robots with Random Time Delays Using Model Predictive Control; In: Gusikhin, O., Madani, K. (eds) Informatics in Control, Automation and Robotics. ICINCO 2018, vol 613. Springer, Cham., 2020; pp 407–428. https://doi.org/10.1007/978-3-030-31993-9_20.

(31) Narakathu, B. B.; Eshkeiti, A.; Reddy, A. S. G.; Rebros, M.; Rebrosova, E.; Joyce, M. K.; Bazuin, B. J.; Atashbar, M. Z. A Novel Fully Printed and Flexible Capacitive Pressure Sensor. In *2012 IEEE Sensors*; IEEE, 2012; pp 1–4. https://doi.org/10.1109/ICSENS.2012.6411354.

(32) Eshkeiti, A.; Emamian, S.; Avathu, S. G. R.; Narakathu, B. B.; Joyce, M. J.; Joyce, M. K.; Bazuin, B. J.; Atashbar, M. Z. Screen Printed Flexible Capacitive Pressure Sensor. In *IEEE SENSORS 2014 Proceedings*; IEEE, 2014; pp 1192–1195. https://doi.org/10.1109/ICSENS.2014.6985222.

(33) Khan, S.; Lorenzelli, L.; Dahiya, R. S. Screen Printed Flexible Pressure Sensors Skin. In *25th Annual SEMI Advanced Semiconductor Manufacturing Conference (ASMC 2014)*; IEEE, 2014; pp 219–224. https://doi.org/10.1109/ASMC.2014.6847002.

(34) Guo, Z.; Mo, L.; Ding, Y.; Zhang, Q.; Meng, X.; Wu, Z.; Chen, Y.; Cao, M.; Wang, W.; Li, L. Printed and Flexible Capacitive Pressure Sensor with Carbon Nanotubes Based Composite Dielectric Layer. *Micromachines (Basel)* 2019, *10* (11), 715. https://doi.org/10.3390/mi10110715.

(35) Shi, H.; Al-Rubaiai, M.; Holbrook, C. M.; Miao, J.; Pinto, T.; Wang, C.; Tan, X. Screen-Printed Soft Capacitive Sensors for Spatial Mapping of Both Positive and Negative Pressures. *Adv Funct Mater* 2019, *29* (23). https://doi.org/10.1002/adfm.201809116.

(36) Kurnaz, S.; Ozturk, O.; Mehmet, A. H.; Guduloglu, U.; Yilmaz, N.; Cicek, O. Flexible Capacitive and Piezoresistive Pressure Sensors Based on Screen-Printed Parylene C/Polyurethane Composites in Low-Pressure Range. *Flexible and Printed Electronics* 2023, *8* (3), 035015. https://doi.org/10.1088/2058-8585/acf774.

For Table of Contents Only

Table of Contents (TOC)/Abstract Graphic